IOP Publishing Eur. J. Phys. 47 (2026) 045603 https://doi.org/10.1088/1361-6404/ae8e0d

European Journal of Physics

RECEIVED
5 May 2026

REVISED
3 July 2026

ACCEPTED FOR PUBLICATION
21 July 2026

PUBLISHED
26 August 2026

PAPER

Sagnac effect, an easy way to a relativistic experiment

Sylvain Fautrat[*]

Retired from Gustave Eiffel University, Champs-sur-Marne, France
[*] Author to whom any correspondence should be addressed.

E-mail: sylfau.xyz@free.fr

Keywords: Sagnac effect, optical fiber interferometer, birefringence, rotating frame of reference in special relativity, theory choice based on numbers

Supplementary material for this article is available online

Abstract

An inexpensive interferometer, in which infrared light travels through ordinary telecommunications optical fiber, is described. In one section of the fiber, two waves travel in opposite directions, so that when the device is rotated, it exhibits the Sagnac effect. A digital display allows direct visual observation, and the effect is even visible when the device is slowly rotated in the hands. The theoretical model is developed and requires only basic knowledge of optics (polarized light, birefringent medium) and special relativity (laws of length contraction and time dilation, laws of velocity composition). The article introduces useful higher-level concepts (rotating frame of reference, comoving frames of reference). The calculations are then carried out in a very concrete experimental context. Quantitative observations are clearly in good agreement with relativistic kinematics and not at all with Galilean kinematics. The interferometer at rest also allows the observation of unusual optical effects.

1. Introduction

We are talking about a *Sagnac interferometer* when two waves travel along the same path containing one or more loops, one wave propagates in one direction, the other in the opposite direction. The *Sagnac effect* is the phase shift that occurs between the two waves when the loop is rotated. In this case, the path is defined by a low-absorbing infrared optical fiber, of the type used in telecommunications. By varying the rotation speed of the loop, the change in phase shift can be quantitatively studied. Conversely, if the relationship between these two quantities is known, determining the phase shift allows us to deduce the rotation speed. This is the principle behind optical gyroscopes.

Furthermore, the light used is polarized and propagates in a birefringent medium exhibiting curvature. For this reason, the apparatus is interesting for its particular optical properties, even if the article title emphasizes the kinematic aspect. The initial motivation is the search for an experimental situation feasible with the most modest means possible, but whose theoretical modeling, to be consistent with observations, requires the framework of Lorentzian kinematics rather than Galilean kinematics. A recent treatise on the Theory of Relativity states « The most interesting aspect of rotation observers is certainly the Sagnac effect » [1].

The assembly replicates, in a simplified form, the basic structure of the high-performance, complex, and expensive fiber optic gyroscopes (FOG) [2, 3]. After simplification, what remains is essentially an interferometer constructed as follows (figures 1–3). A long optical fiber is wound in a number of turns, with its two ends connected to two of the four arms of an X-shaped splitter-coupler. A light source sends a beam into one of the two remaining arms. After splitting, this results in two subbeams, one injected into one end of the fiber coil, the other injected into its other end. The two secondary waves travel through the coil, each in one direction, and return to the coupler. The wave exiting through the fourth arm is a superposition of these two waves. If propagation within the coil creates a phase shift between them, the intensity of the resulting wave depends on this phase shift. The detector that receives

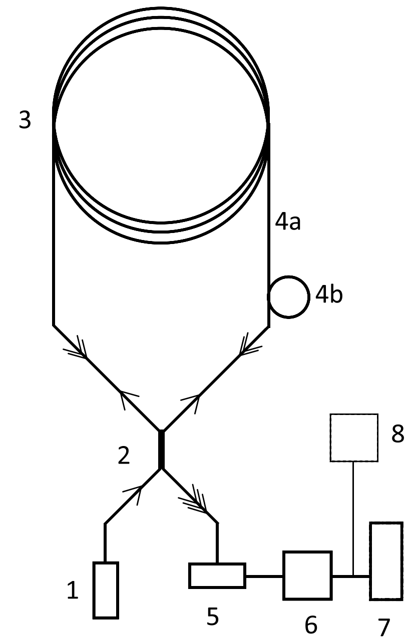

Figure 1. Schematic view of the interferometer showing the components and the paths followed by the two waves after leaving the splitter-coupler then passing through the coil, and passing back through the coupler towards the light detector.
(1) Light source (2) splitter-coupler (3) optical fiber coil (4) polarization modifier: 4a-manipulable section of fiber, 4b-small coil (5) light detector (6) electronic amplifier (7) digital display (8) buzzer (optional).

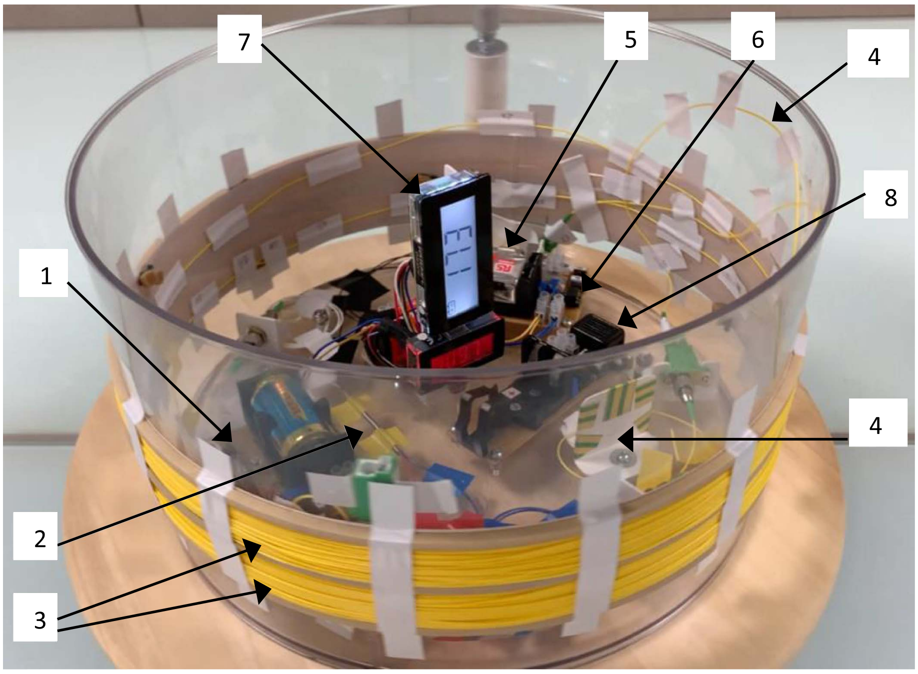

Figure 2. Interferometer seen in perspective. Same captions as figure 1.

this wave is sensitive to the intensity, and the value it displays allows us to track the variations of the phase shift according to the chosen experimental conditions.

The components of the completed device cost approximately 300 euros (350 dollars). The device is hand-sized, and by rotating it, the relativistic evolution of the phase shift can be observed on the display. Conversely, when subjected to pure translation in any direction, the displayed value remains unchanged.

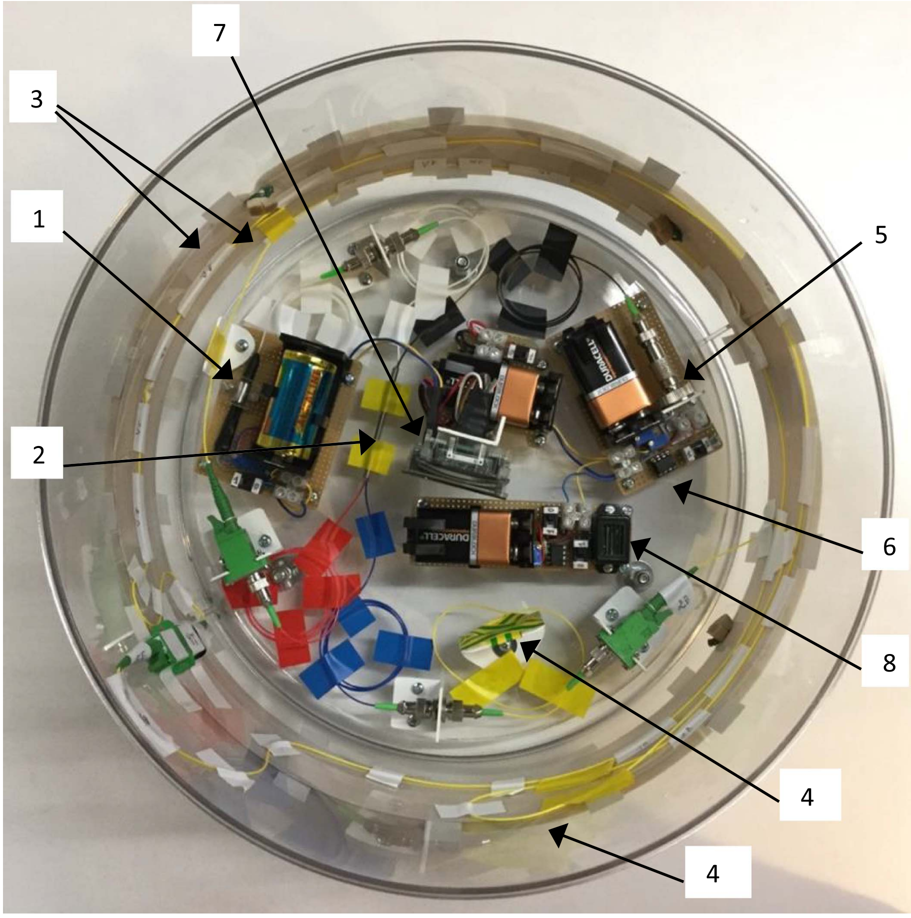

Figure 3. Interferometer seen from above. Same captions as figure 1.

Video 1. Fiber ring interferometer subjected to various translations and rotations
As observed on the central display, the Sagnac effect occurs only when there is rotation about the axis of the yellow fiber coil.
(An animation of this figure is available in the online article.)

With a constant rotational speed, the display shows a constant value. As the rotational speed increases steadily, the displayed value changes, but not continuously. It fluctuates according to a sinusoidal function of the angular velocity, between a minimum and a maximum values. This is indeed consistent with relativistic theoretical analysis.

Furthermore, it is observed that if the shape of the fiber is changed on the device at rest, this has two consequences: the displayed value changes, and, when the device is then rotated, the minimum and maximum values of the sinusoidal variation are also changed.

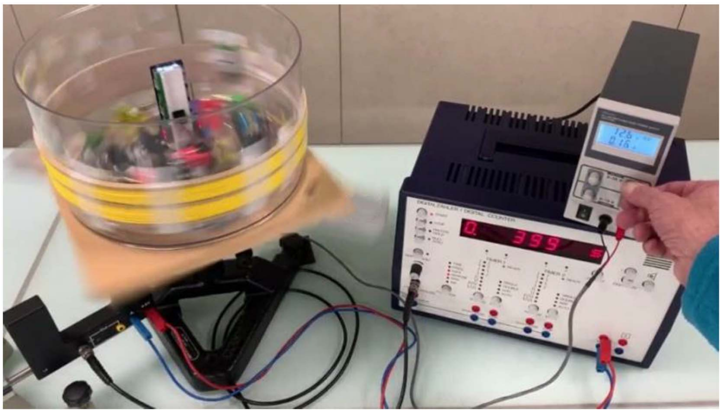

Video 2. Fiber ring interferometer subjected to increasingly rapid rotation
Observation of the display shows that the interference state in the detector evolves cyclically as the rotation speed increases. The displayed value, which is 000 at rest, passes successively through the extrema (visible by freeze frames): 510, 001, 498, 003, then increases again before the rotation is stopped.

(Note that the value on the interferometer is displayed with a certain delay, and that the period value is displayed on the timer with a different delay, which, incidentally, depends on the rotational speed. Thus, the two values seen at a given moment do not correspond exactly to the same state. To obtain representative values, measurements must be taken with each rotation speed held constant for several seconds.)

(An animation of this figure is available in the online article.)

The various observations can be explained based on wave optics in birefringent media and on kinematics, according to the following outlines.

For example, with 200 meters of fiber to travel and a refractive index of approximately 1.5, the propagation time of each of the two waves is about 1 μs. The interference state between the two waves at the detector depends on the precise value of the difference Δt between these two times. A given value of Δt corresponds to a phase difference $\Delta\phi$ between the two waves and corresponds to a certain detected light intensity. However, with this device, the value of Δt can change according to two different processes. First, a change in the birefringent medium can alter the propagation velocities of each of the two waves relative to that medium. Second, the medium can be set in rotational motion relative to the inertial frame of reference in which Δt is considered. In this case, the propagation velocities in this frame of reference are also modified, according to the law of velocity composition. Regarding phase shifts, in the first case we will speak of the optical phase shift $\Delta\phi_{\mathrm{opt}}$, and in the second case of the Sagnac phase shift or kinematic phase shift $\Delta\phi_{\mathrm{kin}}$. In both cases, the theoretical analysis does indeed lead to values for Δt that can be as large as the period of the wave (to optical path differences as large as the wavelength).

The results obtained with rotation are remarkable in that the effects are perfectly observable at a speed as low as 0.1 revolution per second. In this case, the linear speed of the fiber, which is included in relativistic calculations as the speed between frames of reference, is approximately 10 cm s^{-1}. However, this device cannot detect movements as slow as, for example, the Earth's daily rotation. It is optimized with regard to criteria of simplicity, low cost, and demonstrative value, but not with regard to metrological performance. Regarding theoretical analysis, this limited sensitivity has the advantage of allowing the laboratory frame of reference to be considered inertial.

The following section details the construction of the interferometer. In section 3, some observations made with the instrument in a fixed (non-rotating) position are reported and analyzed from an optical perspective. Section 4 is devoted to the experimental results obtained with the rotating instrument and to the theoretical analysis involving kinematics. The phase shift to be considered is essentially that associated with the large fiber length constituting the coil. In appendix A, it is shown that the other fiber elements effectively represent negligible contributions in comparison. Appendix B indicates that, when high measurement accuracy is sought, other physical effects besides those considered in this article must also be taken into account. Some historical background regarding the relativistic interpretation of the Sagnac effect is given in appendix C.

2. The experimental setup

The diagram in figure 1 shows the overall layout of the optical circuit. Photographs in figures 2 and 3 show the device as it was built on a circular platform, which was then attached to the bottom of a transparent cylindrical box approximately 30 cm in diameter. All components, including the power supplies, are mounted either on the platform or on the box, making it a self-contained unit. The various components are detailed below in the order of their numbering in figures 1–3. Technical information on the components used is provided in Note [4].

1) The light source is a laser diode that emits a polarized infrared wave with a wavelength of 1310 nm, commonly used in telecommunications, through a segment of fiber equipped with a connector. It incorporates an optical isolator whose role is to block external light traveling through the fiber towards the diode, as this light would interfere with the laser effect. For monitoring purposes, the source has an electrical output that delivers a voltage that increases (non-linearly) with the emitted power.
2) The beam splitter-coupler acts as a beam splitter operating in both directions of propagation. This type of coupler, made from two parallel fiber sections partially fused over a length of a few millimeters, has two fibers with connectors at each end. When a light beam enters any of the four ports, two secondary waves emerge from the two ports on the other side of the coupler. These secondary waves have a certain phase difference and a certain ratio between their amplitudes. A coupler with a 50/50 (3 dB) ratio is chosen, meaning it produces two equal amplitudes. In this case, one of the two waves is in phase with the incident wave, and the other is in quadrature [5].
3) The optical fiber is wound on the outside of the cylindrical box. There is a first coil consisting of 107 turns with a connector at each end, and above it a second coil of 105 turns. This allows experimentation with a single winding or with both in series. Each turn represents approximately 1 m of fiber.
4) In two places, it is possible to locally modify the shape of the optical circuit. A section of fiber located in line with the first coil can be deformed and moved manually on the cylindrical surface (figures 2 and 3: 4a). A little further along, the fiber is wound in ten turns (approximately 2.5 cm in diameter) on a plate (figures 2 and 3: 4b) which can be rotated around an axis perpendicular to the platform.
5) The detector consists of a PIN photodiode whose signal is amplified by a transimpedance circuit.
6) Amplifier.
7) The two digital displays are digital voltmeters in the 0–200 mV range. The larger one displays a value proportional to the power received by the photodiode. It is positioned with its longest side aligned along the axis of rotation, and thus remains readable up to rotation speeds of approximately five revolutions per second. The smaller one, located below it, is for monitoring the light source and its role is secondary.
8) This is an optional component that emits a sound when the intensity received by the detector exceeds a user-defined threshold. As the interferometer rotates faster, an audience that cannot visually follow the variations on the display can nevertheless hear alternating sounds and silences, indicating that the light intensity received by the detector does indeed follow a cyclical variation (which is consistent with relativistic analysis and inconsistent with classical analysis, as explained later). This function is achieved by applying to the buzzer a fraction of the voltage present on the main display.

Here are some details about the fiber. For all the different segments that make up the optical circuit of the device, the fiber must be single-mode. For the intended use, it is desirable that a wave be clearly identified and not be able to multiply according to several propagation modes by multiple reflections inside the fiber. Fibers developed for telecommunications are high-performance and inexpensive. They are available in single-mode (SMF, for single mode fiber) versions for the wavelength of 1310 nm (1550 nm is another common and usable value). The fiber consists of a core, a cladding, and a primary PVC coating. Their respective diameters are usually 9, 125, and 250 μm. In the following, 'D_{clad}' will refer to the 125 μm diameter of the cladding. An optional secondary coating consisting of a 900 μm diameter tube can provide more effective protection for the fiber. This is the choice that was made here. The refractive index values in the core and in the cladding are close to 1.45 (that of the core being slightly higher than that of the cladding).

All the fiber parts are secured, either to the tray or to the cylindrical box, by means of adhesive strips.

Regarding the use of the device, a few aspects are worth noting.

The detector can display values ranging from 0000 to 1999 with a resolution of 1 unit. To make effective use of this range, one can adjust the laser diode power supply, the photodiode amplifier, or—most commonly—the voltage divider connecting it to the display.

As a general rule, starting from a certain initial displayed value and without any intervention on the interferometer, this value decreases slowly, by 2%–10% per hour depending on the interferometer's configuration (such as the shape and length of the fiber, as well as the initial detected power). Since the detector is located at the end of the circuit, all components are likely to play a role. This observation can be explained by several known phenomena: the heating of the laser diode (which affects the power and degree of polarization), the thermal sensitivity of the various electronic components, and, to a lesser extent, the voltage drop of the battery powering the laser diode. Once identified, this decrease can be taken into account in the analysis of the experiments.

Finally, since temperature is a parameter, the interferometer should be used in a room with a constant temperature.

3. Interferometer at rest

3.1. Experimental observations

With the interferometer at rest, there is no Sagnac effect. Immediately after assembling the device, with one or both coils in series, a certain value is displayed. Then, it can be observed that by manually deforming a portion of the fiber, the value displayed by the detector changes, increasing or decreasing depending on the action performed. One can, for example, try to increase this value as much as possible. Conversely, by manipulating one, or better yet two, different sections of fiber, one can, through successive trials, reduce the displayed value to a very small fraction of the maximum encountered, possibly even obtaining a value of zero.

Video 3. Fiber ring interferometer, at rest, whose fiber is subjected to deformations
As observed on the central display, each of the two ways of deforming the fiber causes a change in the interference state in the detector

(An animation of this figure is available in the online article.)

For comparison, when the same components are assembled without the coupler to create a purely linear optical circuit, where a single wave propagates in only one direction to the detector, deforming the fiber does not cause any change in the displayed value. Deforming a portion of the fiber only has an effect when, within that portion of the fiber, there are two waves propagating in opposite directions. It will be shown later that this effect can be explained by taking into account the polarization of each wave as well as the birefringence induced in the propagation medium.

The following sections are devoted to explaining the effects of fiber deformation.

3.2. Information on fiber birefringence induced by curvature and twist

Glass, initially amorphous silica, becomes birefringent [6] when its microscopic structure is modified by external stresses of a mechanical, thermal, or electromagnetic nature. For a fiber, opportunities for mechanical stress exist from the production process itself (passage through die, contraction upon cooling, stretching, etc). When the fiber is bent to be wound around the 30 cm cylinder, it undergoes anisotropic deformations, with strong stresses along its longitudinal axis (compression on the inner side of the bend and stretching on the outer side) and weak stresses along the other two directions. This results in linear birefringence where the extraordinary axis lies in the plane of curvature and the ordinary axis is perpendicular to the plane of curvature. A wave with either of these particular polarization directions propagates without the medium causing rotation, in one direction or the other, around the direction of propagation. Thus, a wave entering a circular section of fiber with a polarization located in the plane of curvature will travel along the section with a certain speed, its polarization direction remaining in that plane (extraordinary propagation mode). A polarization perpendicular to the plane of curvature will also remain in this way, but with a different speed (ordinary propagation mode). A wave entering with any polarization direction is to be considered as a combination of its two components relating to the two particular modes.

In the case of silica, the ordinary axis is the slow axis, with a path difference that depends on the diameter D of the loop according [7] to:

$$\Delta n \approx 0.133\left(\frac{D_{\mathrm{clad}}}{D}\right)^2. \tag{1}$$

Thus, an ordinary wave and an extraordinary wave, traveling through a circular loop of length πD, acquire a path difference $\Delta n(\pi D) \approx 0.133(\pi D_{\mathrm{clad}}{}^2/D)$. For 100 turns of a fiber coil, with a diameter $D = 30$ cm, $D_{\mathrm{clad}} = 125\ \mu$m, $\lambda = 1310$ nm, the path difference is therefore approximately 21 μm $\approx 16\lambda$. For the turns of the polarization modifier, of diameter $D = 2.5$ cm, the path difference is approximately 2λ.

In conclusion, when a circuit like that of the interferometer is traversed by two waves of different polarizations, their interference state at the output generally depends very strongly on the birefringent nature of the propagation medium.

In addition to curvature, the fiber can generally undergo some twisting during winding or installation on the interferometer platform. The mechanical stresses associated with twisting induce circular birefringence. In this case, a linearly polarized wave entering a twisted section has its polarization direction that rotates as it propagates, in one direction or the other depending on the direction of the twist in the medium. At the output, the polarization direction has rotated by an angle of approximately $0{,}07.\theta_{\mathrm{twist}}$, where θ_{twist} is the twist angle of the medium along the entire section [8]. For example, a 90° twist in a portion of the fiber generates a 6° rotation of the polarization.

3.3. The effects of a change in fiber shape on each of two waves

Figure 4 shows two schematic versions, (a) and (b), of the interferometer. The two optical circuits are practically identical and located in the XY plane, with the exception in case (b) of the portion between $D1$ and $D3$, which lies in the XZ plane. Consider a wave exiting the source with a polarization direction along Z. It then passes through the curvature at A according to the ordinary propagation mode, and the two secondary waves exiting the coupler are therefore also polarized along Z.

In case (a), the secondary wave passing through the bends at B, C, D1, D2, E, F, and G propagates in ordinary modes and reaches the detector with Z-polarization. The same is true for the other secondary wave passing through F, E, D2, D1, C, B, and G. Finally, at the coupler, both waves are Z-polarized. Furthermore, they have followed the same geometric path in the fiber, and the two optical paths must be calculated for both waves with the same ordinary refractive index values at the different points. Their phase shift has therefore remained the same as at the coupler output.

In case (b), the secondary wave passing through B and C propagates in ordinary modes and approaches $D1$ with Z-polarization. This direction lies in the XZ plane of the curvature at $D1$, hence an extraordinary propagation mode. The polarization therefore rotates in this XZ plane and becomes parallel to X. It is thus in the XZ curvature plane of the curvature at $D2$, where it rotates 180° to become parallel to X again. For the curvature at $D3$, it is an ordinary mode that maintains the X direction. Afterward, the curvatures up to the detector are all in the XY plane, the modes are all extraordinary, and after three 90° rotations in this plane, the polarization is in the Y direction at the detector. The other secondary wave passes through F and E in ordinary modes. It therefore approaches the curvature at $D3$ with Z-polarization, resulting in an extraordinary mode that rotates it to become parallel to Y. Propagation through the curvatures at $D2$ and $D1$ consists of ordinary modes that maintain the $\underline{Y}$ direction. The subsequent curvatures up to the detector are all in the XY plane, the modes are all extraordinary, and the polarization is along Y in the detector. Finally, at the coupler, both waves are Y-polarized. This time, for most of the geometric path, the two optical paths must be calculated using ordinary index values for one secondary wave and extraordinary index values for the other.

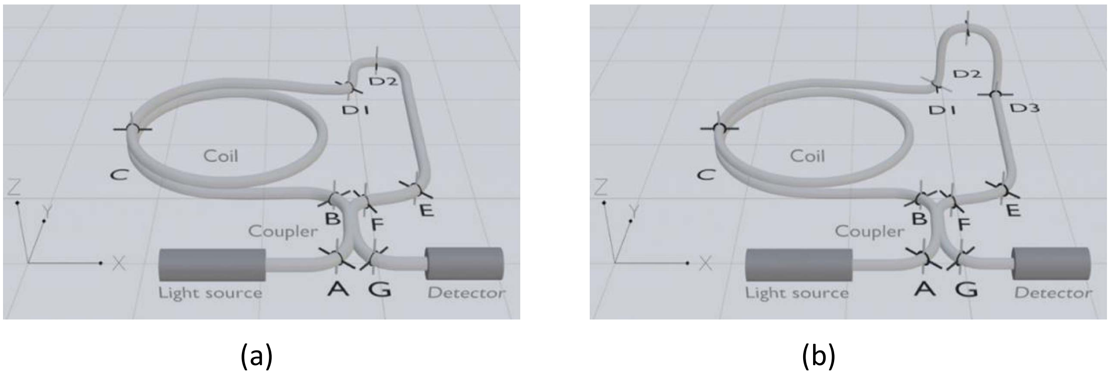

Figure 4. Two circuits having geometric shapes that differ only in the sections marked with the letters D. The optical fiber in circuit (a) follows a curved line that lies practically entirely within the XY plane. Circuit (b) is obtained when the section between $D1$ and $D3$ lies in the XZ plane. Points A–G mark regions where the fiber is curved and therefore birefringent. For each of these points, the ordinary axis of birefringence is indicated by a light gray segment, and the extraordinary axis by a black segment.

In both cases, two secondary waves travel through the circuit beyond the beam splitter and then reach the detector. The difference in shape between the two circuits impacts the polarizations and the phase shift of the two waves at the detector. This impact is explained in section 3.3.

Based on the orders of magnitude in the previous section, the resulting path differences can easily exceed the wavelength. The phase shifts of the two waves at the detector in case (a) and in case (b) can therefore be significantly different. This is all the more true since the effects of changes in polarization direction due to twisting can be superimposed on the effects of curvature. This particular circuit illustrates how, in general, a change in shape can indeed modify the polarization directions and the phase difference of the two waves received by the detector, and consequently alter the received light power.

From an experimental point of view, it is noted that manipulating the shape of the fiber is a practical way to modify the interference state at the detector level [9].

3.4. Expression of the received light intensity as a function of the phase shift

In general, the intensity at the detector is determined by the amplitudes of the two waves, the angle between their polarization directions, and their phase shift. Theoretical tools such as Jones matrices exist to account for the evolution of these quantities during propagation through a succession of birefringent media. However, applying these tools to a specific interferometer, which accurately incorporates the detailed characteristics of all the material components and their junctions, is difficult [10]. Furthermore, for the upcoming study, we only need a general expression for the intensity that encompasses the different possible configurations with regard to amplitudes, angle between the two polarization directions, and phase shift $\Delta\phi$ between the two waves, regardless of its origin. With the interferometer at rest, the phase shift is associated with the optical path difference along the path where both waves are present: the splitter-coupler, the coil, the polarization modifier, and the rest of the circuit up to the detector. When the interferometer rotates, $\Delta\phi$ can also have a kinematic component. Starting from the well-known expression for the case of interference between two scalar waves of the same frequency, we derive the following expression:

$$A[1+\cos(\Delta\phi)]+B. \tag{2}$$

The polarization states of the two waves, and their possible amplitude difference, are accounted for by the parameters A and B. For example, a non-zero angle between the two polarization directions implies a non-zero value for the intensity regardless of the phase shift; this is permitted by a non-zero value for B.

When zero is displayed, it means the two waves cancel each other out; they have the same polarization direction and amplitude, and are in antiphase. For the parameters of equation (2), this corresponds to:

$$\begin{aligned}\Delta\phi &= \pi,\\ B &= 0.\end{aligned} \tag{3}$$

Since the received power is the integral of the intensity over the detector surface, a change in intensity results in a change in power, and consequently, a change in the value V displayed by the detector. V

is proportional to the power by a factor that depends on the amplification of the photodiode signal and on the fraction of voltage subsequently applied to the display. In our experimental context, the displayed value V is the accessible quantity. Therefore, for the analysis of an experiment performed with constant interferometer settings, the mathematical form of equation (2) will be used for V. However, we should avoid comparing V values corresponding to different experimental conditions (length and shape of the fiber, voltage applied to the laser diode, various settings of the electronics, etc).

4. Rotating interferometer

4.1. Experimental results

The interferometer is mounted on a rotating table that imposes different rotational speeds. The speed is determined from an electronic counter that measures the average period over two successive rotations. Although the counter resolution is 1 μs, taking into account the light barrier fork that triggers it, we use 1×10^{-3} s^{-1} as the uncertainty in the rotational speed. The value V to be recorded on the detector during the rotation is read directly by eye.

Before rotation begins, depending on the settings on the interferometer at rest, a certain positive or zero value is displayed. When rotation starts, depending on the direction of rotation, the value may increase or decrease (if it was not zero).

Video 4. Fiber ring interferometer rotated in both directions, starting from the value 001 displayed at rest
When rotated, the displayed value increases in the same manner in both directions.
(An animation of this figure is available in the online article.)

Video 5. Fiber ring interferometer rotated in both directions, starting from the value 249 displayed at rest
In this example, when rotated, the displayed value increases in one direction and decreases in the other.
(An animation of this figure is available in the online article.)

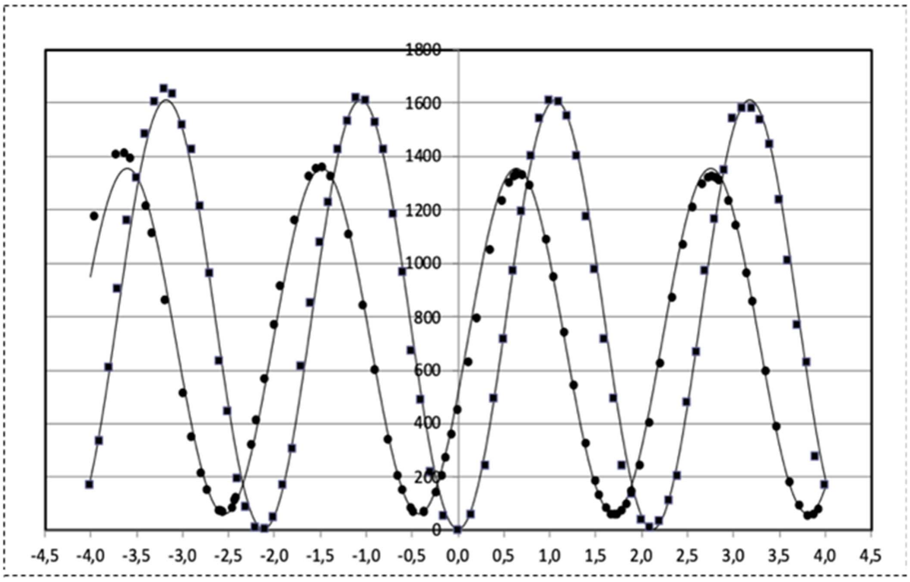

Figure 5. With the interferometer rotating, two series of V values recorded on the detector display as a function of the rotation speed N in revolutions per second. The fiber coil used is the one with 107 turns. For the series of square marks, the interferometer was set to display zero at rest. For the series of round marks, it displayed the value 450. In the second case, the value increases when rotating in one direction and decreases in the other direction. The two series are well approximated by the two sinusoidal curves (described in section 4.1).

Then, as the rotation speed N increases, the displayed value V varies according to a nearly sinusoidal law. Figure 5 shows two typical sets of readings with the 107-turn fiber coil.

During measurements, each time the rotation speed is changed, a short delay is required for the displayed value to stabilize. There are several reasons for this: the mechanical inertia of the rotating platform; the stopwatch used only updates the rotation period after two complete revolutions; and the detector display has a response time of almost one second. Consequently, recording a sufficiently detailed series of values takes nearly an hour. This explains the gradual decrease in V observed in figure 5, a phenomenon already noted with the interferometer at rest.

The two sinusoidal curves in figure 5 are obtained from equation (2) using a two-component phase shift. The kinematic term is proportional to the rotational speed N to account for the periodic nature of the data:

$$V = A\left(1+\cos\left(\Delta\phi_{\text{opt}}+\frac{2\pi N}{\Delta N}\right)\right)+B \tag{4}$$

where ΔN is the difference in rotational speed (on the x-axis) between two successive minima or two successive maxima.

ΔN can be experimentally evaluated from independent measurements, specifically those of the extrema. On the one hand, pinpointing an extremum can be relatively precise, and on the other hand, the time required to record all the maxima over the accessible range of rotational speeds is much shorter, thus with more stable electronic components. To increase the precision of ΔN, the average value calculated over the entire range is used. Figure 6(a) shows two such series of measurements with the 105-turn fiber coil, and figure 6(b) shows two series with the two coils of 107 and 105 turns in series. Based on the data in the caption of figure 6, we can consider that ΔN between two successive extrema does not depend on the interferometer settings at rest. However, ΔN depends significantly on the number of fiber turns. For the remainder of the study, we retain the value $\Delta N = 2.117$ rev s^{-1} for the 107-turn coil, and the value $\Delta N = 1.063$ rev s^{-1} for the two coils in series. The first of these two values was used to apply equation (4) to the series in figure 5 to obtain the two sinusoidal curves. The other parameters A, B, and $\Delta\phi_{\text{opt}}$ were also evaluated without resorting to a statistical algorithm. For B, we take the average Vmin of the three or four minimum values of V found among the experimental readings. For the amplitude A of the sinusoid, we take (Vmax−B)/2, where Vmax is the average of the four maximum values of V [11]. Furthermore, for the series where $V = 0$ at rest, $\Delta\phi_{\text{opt}}$ equals π (see equation (3). Its value for the other series is adjusted manually so that the curve closely approximates the marks of the series.

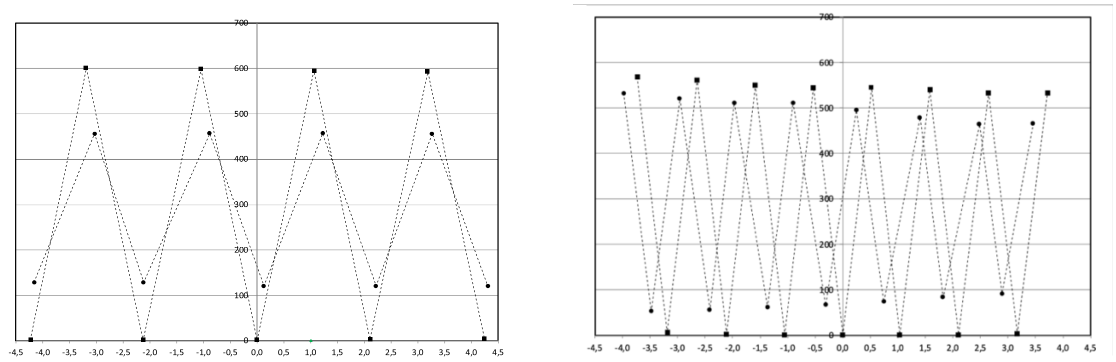

(a) (b)

Figure 6. With the interferometer rotating, the values V recorded on the detector display as a function of the rotation speed N in revolutions per second (rev s^{-1}).

Only the extrema are sought. Square marks correspond to a zero value V on the interferometer at rest, and round marks to a non-zero value.

(a) The fiber coil used is the one with 107 turns. The parameter ΔN is the difference between two successive extrema. For each of the two series, it is calculated as the average value derived from the rotational speeds of the first minimum and the last minimum. The result is 2.118 rev s^{-1} for the square marks and 2.116 rev s^{-1} for the round marks.

(b) The two coils with 107 and 105 turns are connected in series. Taking into account the maxima this time (which are more numerous than the minima), the calculation of ΔN yields 1.064 rev $s^{-1}$for the square marks and 1.062 rev s^{-1} for the round marks.

4.2. Modeling for the theoretical determination of the Sagnac phase shift

With the interferometer rotating, the two secondary waves are in the conditions where the Sagnac effect occurs, namely the appearance of a kinematic phase shift between them. We then expect that a theoretical account of this effect will provide an explanation for the periodic nature of the variation observed at the detector, and if possible, give a quantitative expression for the periodicity in ΔN.

We denote K the inertial reference frame of the laboratory relative to which the interferometer is rotating at rotational speed N. Let K_0 be the rotating frame of reference with respect to which the interferometer is at rest, and let ν_0, or more simply ν, be the frequency of the emitted wave. In general, if the two secondary waves of the same frequency $\underline{\nu}$ travel along any segment of fiber, identified in K_0, in times that differ from each other by Δt_0, the resulting phase difference between the waves is written as:

$$\Delta\phi = 2\pi\nu\Delta t_0. \tag{5}$$

To represent each wave in calculations, we can consider a moving point corresponding to a given phase value (for example, a wave crest) traveling at the phase velocity. The phase velocity V in a medium, or the refractive index $n = c/V$, are measured relative to the rest reference frame of the medium, so here K_0. The same applies to the emission frequency of the source.

To denote the quantities relating to the wave propagating in the same direction as the rotation of the interferometer with respect to K, the subscript $+$ is used, and the subscript—for the wave propagating in the opposite direction. Thus, the velocities are denoted v_{0+} and v_{0-} for K_0, and v_+, v_- for K. One can also refer to the difference $\Delta n = n_+ - n_-$ between the two refractive indices corresponding to v_{0+} and v_{0-}.

The fiber coil is treated in calculations as a cylinder of radius R_0 and negligible height.

We will now consider the 'classical' Galilean framework and then the 'relativistic' Lorentzian framework.

4.3. Hypothesis of classical (Galilean) kinematics

With respect to the non-inertial reference frame K_0 linked to the interferometer, the study is immediate.

The geometric length L to be traveled is the same for both waves. The time difference is given by $\Delta t_0 = \frac{L}{v_{0+}} - \frac{L}{v_{0-}} = \frac{L}{c}\Delta n$. There is no difference concerning the interferometer, whether it is at rest or rotating. The phase difference $\Delta\phi = 2\pi\,\nu\,\Delta t_0$ corresponds only to the optical phase shift and there is no kinematic term. The periodic dependence on the rotational speed observed experimentally is not found at all. The assumption of classical kinematics is not compatible with the observations. We can also reason in the laboratory frame, with the propagation speeds v_+ and v_- obtained from the law of composition of velocities, but we arrive at the same conclusion.

In the special case where the two velocities are equal, $v_{0+} = v_{0-} = v_0$, we obtain $\Delta\phi = 0$ [12–14].

4.4. Hypothesis of relativistic (Lorentzian) kinematics

Calculation method

The reference frame K_0 is defined by the plane of the interferometer's rigid platform, its axis of rotation, and its rotational speed relative to K. However, this does not reveal the very specific geometric and temporal characteristics of this type of non-inertial reference frame. Within the framework of special relativity, the study of the rotating disk [15], for example, shows that the perimeter measured on the disk itself is larger than that measured in the laboratory frame [16]. A proof of this result is given below and serves as an introduction to the subsequent calculations. Another result concerns time: while neighboring clocks on the disk can indeed be synchronized locally, clocks distributed globally along a closed curve cannot all be synchronized, unlike the case of clocks in an inertial reference frame. To address the issue of a frame of reference such as a rotating disk, a simple method consists of decomposing any process distributed on the disk into a set of elementary processes, each carried out on a length scale $\mathrm{d}l_0$ around a point M_0 and on a time scale $\mathrm{d}t_0$ around a time t_0. For each of the elementary processes, we introduce the comoving inertial frame K' of M_0 (the 'instantaneous tangent inertial frame') which serves as an intermediary. Locally, the kinematic quantities (length, time, velocity) have the same values in K_0 and K'; and between K' and K, they are related by the usual relativistic laws given by the Lorentz transformation or laws derived from it. This procedure allows us to transpose a global study into the inertial frame K, for which there are no difficulties related to globality.

Figure 7 show the interferometer, as viewed from the K_0 reference frame and from the K reference frame, with different geometric parameters, wave kinematic parameters, and various notations that are used below. In K, the velocity vector of the elementary segment of length $\mathrm{d}r$ is at all times perpendicular to the segment itself. Under these conditions, the length of the segment has the same value in K and in its comoving reference frame, and therefore the same value in K_0: $\mathrm{d}r = \mathrm{d}r_0$. The same applies to all segments constituting any radius ($r = r_0$) and in particular to the radius of the disc: $R = R_0$. For the elementary circumferential segment, its velocity vector is parallel to it. Under these conditions, we go from the length of the segment in K to its proper length in K' and K_0 by multiplying by the Lorentz factor (law of proper length contraction) [17]:

$$\mathrm{d}l_0 = \gamma \mathrm{d}l, \tag{6}$$

$$\text{with } \gamma = \frac{1}{\sqrt{1 - \left(\frac{2\pi NR}{c}\right)^2}} \tag{7}$$

The same applies to all the constituent segments of the circumference of the disk, with the same value for γ. Thus, since in K the overall value of the perimeter is $2\pi R$, in K_0 its value is $\gamma 2\pi R$.

The fiber coil

We now want to calculate the phase shift between the two secondary waves for the case of the path of the circular turns of the fiber coil. We consider to begin with the case of the circumferential segment of length $\mathrm{d}l_0$, identified in figures 7(a) and (b).

Figures 7(c) and (d) show the distances traveled in K by each of the two waves. The two relationships written in the captions of these figures can be combined in the following form:

$$\mathrm{d}t_{\pm}\left(v_{\pm} \mp 2\pi NR\right) = \mathrm{d}l. \tag{8}$$

The two wave velocity vectors (of magnitude $\mathrm{v}_{0\pm}$) are respectively parallel and antiparallel to the velocity vector of the comoving frame K' of the segment in question (of magnitude $2\pi NR$). Under these conditions, the relativistic composition of velocities for both cases is written in the form [18] (all quantities being positive):

$$\mathrm{v}_{\pm} = \frac{v_{0\pm} \pm 2\pi NR}{1 \pm \left(\frac{v_{0\pm}.2\pi NR}{c^2}\right)}. \tag{9}$$

From equations (7) and (8), we obtain the following expressions for the durations:

$$\mathrm{d}t_{\pm} = \gamma^2 \mathrm{d}l\left(\frac{1}{v_{0\pm}} \pm \frac{2\pi NR}{c^2}\right) \tag{10}$$

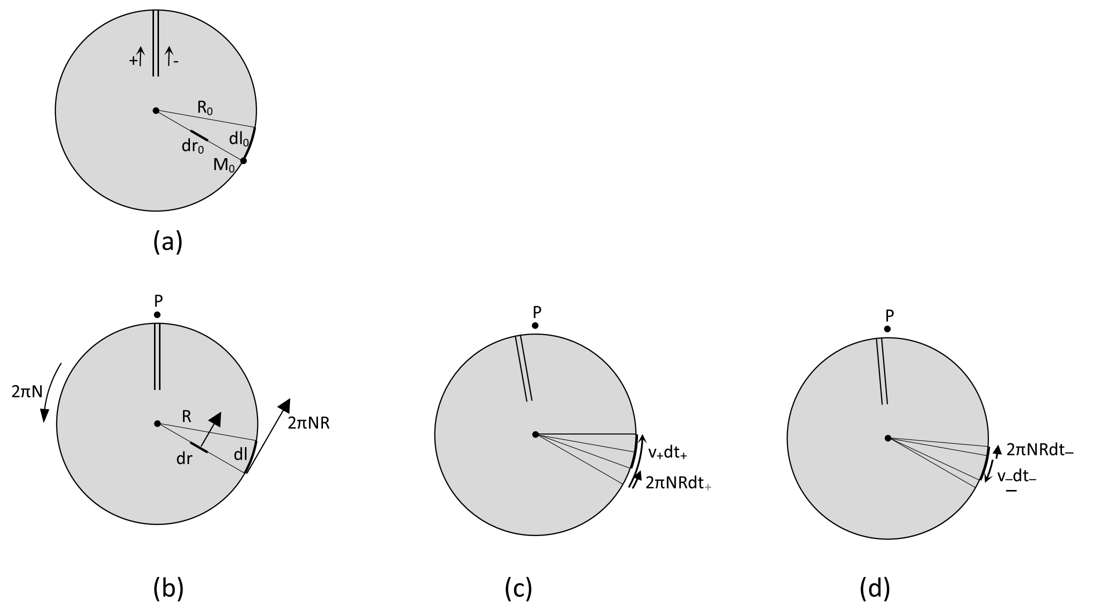

Figure 7. The interferometer as seen from (a) the K_0 reference frame, where it is at rest, and from (b)–(d) the K reference frame of the laboratory. The contour is a circular fiber loop extended by two straight segments aligned along a radius of the disk. The various defined parameters are used for the geometric analysis and the study of wave propagation.
(a) The indications are those relative to the reference frame K_0. The two arrows show the directions of circulation (denoted + and –) of each of the two secondary waves. R_0 is the radius of the disk. On the circumference, M_0 is any point and $\mathrm{d}l_0$ is the infinitesimal length of a segment. $\mathrm{d}r_0$ is the infinitesimal length of a segment aligned on a radius and located at a certain distance r_0 from the center.
(b) The indications are those relative to the laboratory frame K with respect to which the interferometer is rotating at an angular velocity of $2\pi N$. P is a fixed point of K. The radius of the disk measured in K is denoted R. The lengths of the two segments are denoted $\mathrm{d}l$ and $\mathrm{d}r$.$2\pi NR$ is the velocity of point M_0 with respect to K, and the arrow represents the velocity vector of this point, which is also the translation vector of the instantaneous comoving frame K' associated with M_0.
(c) Relative to the laboratory frame of reference, the wave + (which travels in the same direction as the rotation of the disk) travels along the fiber segment of length $\mathrm{d}l$ in a certain time denoted $\mathrm{d}t_+$. During this time, the segment itself moves by $2\pi NR\mathrm{d}t_+$, and the wave (a phase point of the wave), with velocity v_+, moves by $v_+\mathrm{d}t_+$. We see that we have: $v_+\mathrm{d}t_+ - 2\pi NR\mathrm{d}t_+ = \mathrm{d}l$.
(d) Relative to the laboratory frame of reference, the wave—(which travels in the opposite direction to the rotation of the disk) travels along the segment of length $\mathrm{d}l$ in a certain time denoted $\mathrm{d}t_-$. During this time, the segment itself moves by $2\pi NR\mathrm{d}t_-$, and the wave, with velocity v_-, moves by $v_-\mathrm{d}t_-$. We see that here: $v_-\mathrm{d}t_- + 2\pi NR\mathrm{d}t_- = \mathrm{d}l$.

This gives the following difference $\mathrm{d}t = \mathrm{d}t_+ - \mathrm{d}t_-$ between the two travel times in K:

$$\mathrm{d}t = \gamma^2 \mathrm{d}l \left(\frac{1}{v_{0+}} - \frac{1}{v_{0-}} + \frac{4\pi NR}{c^2} \right). \tag{11}$$

By introducing the difference $\Delta n = n_+ - n_-$, we obtain:

$$\mathrm{d}t = \frac{\gamma^2 \mathrm{d}l}{c} \left(\Delta n + \frac{4\pi NR}{c} \right). \tag{12}$$

The corresponding time $\mathrm{d}t_0$ in K' or K_0 is measured locally, that is to say it is a proper time, related to $\mathrm{d}t$ by a Lorentz factor (law of proper time dilation) [19]:

$$\mathrm{d}t = \gamma \mathrm{d}t_0. \tag{13}$$

With equations (6) and (13), equation (12) becomes:

$$\mathrm{d}t_0 = \frac{\mathrm{d}l_0}{c} \left(\Delta n + \frac{4\pi NR}{c} \right). \tag{14}$$

For the case of traversing several turns, the sum of the differences in elementary durations $\mathrm{d}t_0$ reduces, up to a constant factor, to the sum of the lengths $\mathrm{d}l_0$. For each turn, this sum equals $\gamma 2\pi R$, therefore, denoting B as the number of turns, we obtain

$$\Delta t_0 = \frac{\gamma 2\pi RB}{c} \left(\Delta n + \frac{4\pi NR}{c} \right). \tag{15}$$

And according to equation (5), the phase shift is:

$$\Delta\phi = \frac{\gamma 4\pi^2 RB\nu}{c}\left(\Delta n + \frac{4\pi NR}{c}\right). \tag{16}$$

This result warrants several comments. Regarding the factor γ, its dependence on the rotational speed is entirely negligible numerically. For example, for $N = 3$ rev s^{-1}, it differs from 1 by only 5×10^{-17}. Furthermore, the two terms in parentheses clearly correspond to optical and kinematic contributions, respectively. A numerical comparison can be made between the two terms for a given typical situation. For the fiber radius of curvature $R = 15$ cm, equation (1) gives an induced birefringence $\Delta n \approx 2.3 \times 10^{-8}$. The second term in parentheses, with $R = 15$ cm and $N = 3$ rev s^{-1}, is approximately 2.0×10^{-8}. Thus, the kinematic term effectively describes an effect comparable to that of the optical term [20]. The remarkable characteristic of this kinematic term is its independence from the physical nature of the two waves, their speeds, or their polarization directions. Relativistic kinematics leads to such a phase difference whenever there are two waves A and B, of the same frequency, propagating in opposite directions in a rotating medium.

The other fiber parts

One might wonder to what extent the fiber segments that are not part of the coil but nevertheless rotate on the platter exhibit significant kinematic phase shifts. In the previous calculation, the fiber had both a large length and an orthoradial orientation relative to the axis of rotation for each of its length elements. For the other parts of the fiber, one or the other of these conditions, or both, are not satisfied. It is shown in appendix A that their contributions are indeed negligible in comparison, so that the phase shift to be taken into account for the entire interferometer is essentially given by equation (16).

Calculating the periodicity in relation to the rotational speed

The kinematic term of equation (16) is indeed proportional to the rotational speed, as is that of the empirical formula in equation (4). By identifying the two kinematic terms of these two formulas, we obtain the following expression for the periodicity ΔN of the light intensity:

$$\Delta N = \frac{c^2}{8\pi^2 R^2 B\nu}. \tag{17}$$

The number of turns of each of the two coils is known: $B_1 = 107$ and $B_2 = 105$.

To create each coil, the fiber was wound around the cylindrical box to a specific height and thickness. To determine the effective diameter at mid-height of each coil, the inner and outer diameters are measured, and the mean value is taken. This yields the following radii: $R_1 = 0.1482$ m and $R_2 = 0.1490$ m (the box is slightly conical, which explains the difference between the two radii). The frequency is determined from the wavelength in a vacuum ($\nu = c/\lambda$), with $\lambda = 1310$ nm for the laser diode [21].

For the 107.0-turn coil, we obtain $\Delta N_1 = 2.119$ rev s^{-1}, which can be compared to the value obtained from the current extremes: 2.117 rev s^{-1}. For the two coils in series, the two kinematic phase shifts are added together, which corresponds, for the periodicities, to an addition of their inverses. With $\Delta N_2 = 2.135$ rev s^{-1} for the 105.0-turn coil, this gives $\Delta N_{1+2} = 1.063$ rev s^{-1}, which can be compared to the value obtained from the current extremes: 1.063 rev s^{-1}. Since these various values were obtained independently of one another, such agreement between them numerically demonstrates the validity of the choice of the physical theory used. The experiments reported here are limited in number, but the results are quite representative (the ΔN values obtained with different fiber configurations—whether using one or two turns—differ by no more than 0.5%).

Finally, note that while in equation (16) the term in parentheses is on the order of 10^{-8}, the phase shift is indeed on the order of one radian, thanks to the values of the frequency and the number of turns, which are factors in the equation.

5. Conclusion

Sagnac effect can be obtained nowadays with modest experimental equipment. The light source, the propagation medium, and the detector are all attached to the same platform. Each portion of the medium constitutes a frame of reference with respect to which the speed of light is well-defined. The theoretical model based on Lorentzian kinematics is in good quantitative agreement with the observations, unlike that based on Galilean kinematics. When the Sagnac effect is involved, even with low instrument speeds, Relativity becomes the essential framework for interpretation. A comment can be made on this point. The kinematic contribution to the phase shift owes its existence to the denominator that is not equal to one in the law of velocity composition (equation (9)). However, this denominator is introduced into the proof of the law as the time derivative of one of the reference frames with respect to the time of the other reference frame. Indeed, when the interferometer is rotated and the numbers scroll across the display, one can say that it is the relativity of time (of time intervals) that is manifesting itself.

The relativistic interpretation of the Sagnac effect has been a subject of controversy in the past and can still be at times. In most historical experiments, light propagated in a vacuum or air, with a refractive index of one in practice. However, by setting the speed of light to c in the laboratory frame of reference, modeling based on Galilean kinematics leads to an expression for the phase shift that is practically identical to the relativistic kinematic term (note that the latter is identical for a vacuum or a medium since it does not depend on speeds). More precisely, the relativistic formula also includes a Lorentz factor, but it is not significant for laboratory experiments. On the contrary, as we have seen, with propagation in an embedded fiber with a refractive index other than one, the Galilean and Lorentzian results are clearly different.

In a fiber-optic interferometer, the phase shift increases with the number of turns of fiber in the coil. It is therefore possible to build devices that are extremely sensitive to rotation based on this principle. Today, angular velocities as low as 1×10^{-4} degree per hour can be detected [22]; for example, this provides a valuable reference orientation for a submarine's blind navigation. However, moving from a simple interferometer to a precise measuring device is not straightforward. Optical fibers are nevertheless subject to a variety of physical effects that tend to limit their performance [23]. Taking these effects into account and optimizing performance requires a wide range of scientific and technological expertise, resulting in complex devices. Information on this topic can be found in the specialized literature [24].

The device considered in this article is subject to different constraints: easy manual manipulation, direct visualization of the effect of rotation, a small number of accessible components, and sufficient precision for theoretical argumentation. Depending on individual preferences, here are some possible variations: a 250 μm diameter fiber without external protection; 'quick cold connections' between fiber elements; a servo-controlled laser power supply to stabilize the emitted power; automated data acquisition (while maintaining direct reading on a display).

This interferometer can be used for teaching in various ways.

From the theoretical standpoint, it can be presented as an example of the application of non-inertial reference frames in relativity, in a context that is tangible for students. Depending on the curriculum, this may apply to either the undergraduate or graduate level. These concepts are rarely covered in introductory textbooks, which gives the impression that Special Relativity deals only with inertial reference frames. This example also demonstrates that there are indeed cases where velocities are low and where relativity is necessary. In practice, it can first be shown in operation to students, then give rise to a theoretical analysis by the teacher, or serve as a case study for exercises combining theoretical understanding and application calculations. The concepts typically involved are polarized waves, interference, birefringence in the case of a curved fiber, for optics, and the composition of velocities, non-inertial frames of reference, co-moving frames of reference, for the theory of relativity.

On the experimental side, the device can, for example, be operated as described in sections 3.1 and 4.1. Determining the periodicity ΔN is straightforward and can be performed with various fiber shapes (with the possibility of statistical analysis). Comparison with the value of ΔN obtained independently from the coil description (equation (17)) then demonstrates that the theoretical framework used exhibits strong numerical agreement with observations. Moreover, this could be the subject of a comprehensive discussion encompassing all relevant uncertainties.

Furthermore, as part of a supervised individual project, students can build the various modules that make up the interferometer.

Data availability statement

The data that support the findings of this study are available in the following two files.

Supplementary data 1 available at: https://doi.org/10.1088/1361-6404/ae8e0d/data1.

Supplementary data 2 available at: https://doi.org/10.1088/1361-6404/ae8e0d/data2.

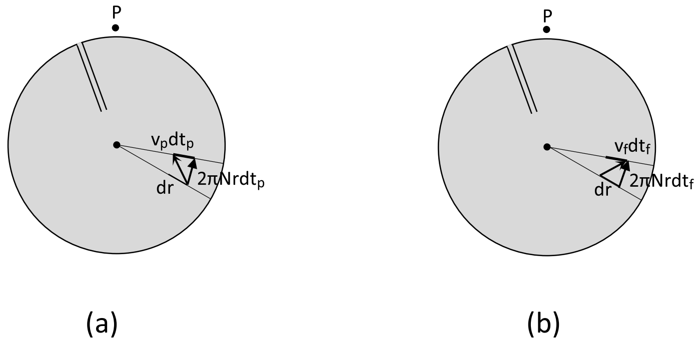

Figure 8. The interferometer as seen from the laboratory reference frame K, with the parameters relating to the propagation of centripetal and centrifugal waves along a radius of the platform.
(a) The wave, denoted p (centripetal), propagates in the fiber segment of length dr In the laboratory frame K, its velocity is denoted v_p. It travels along the segment in a certain time denoted dt_p. During this time, the segment (with velocity $2\pi Nr$) moves by $2\pi Nr$dt_p and the wave moves by v_pdt_p. The fiber segment and its velocity vector are perpendicular at all times. The wave velocity vector and the associated displacement each have a radial component and an orthoradial component.
(b)The wave, denoted f (centrifugal), propagates along the fiber segment of length dr. Its velocity in the laboratory frame of reference is denoted v_f. It travels along the segment in a certain time denoted dt_f. During this time, the segment (with velocity $2\pi Nr$) moves by $2\pi Nr$dt_f, and the wave moves by v_fdt_f. The wave velocity vector and the associated displacement each have a radial component and an orthoradial component.

Appendix A. Phase shifts in fiber sections outside the coil

We seek to evaluate the kinematic terms of phase shift for other parts of the optical circuit where both secondary waves circulate.

- After winding the number of turns of the fiber, the excess fiber was placed against the cylindrical wall of the interferometer in a U-shape, meaning that half of the excess was wound in one direction and the other half wound back. For the return journey, both the A and B waves reversed their direction of propagation relative to the rotation, so the kinetic term retained its value but with the opposite sign. Consequently, for the back and forth trip, the kinematic contribution to the phase shift is zero.
- We now consider a fiber segment of infinitesimal length $\mathrm{d}r = \mathrm{d}r_0$, exactly aligned with a radius of the disk. The task again is to determine, in K_0, the difference between the propagation times of the two waves through the segment. Figure 8(a) shows the case of the centripetal wave (denoted p) and figure 8(b) of the centrifugal wave (denoted f). In the disk's frame of reference, the two phase points have their velocity vectors (with respective magnitudes v_{0p} and v_{0f}) aligned with the fiber, which is radially oriented. This direction is perpendicular to the velocity vector (with magnitude $2\pi Nr$) of the fiber segment in the laboratory frame of reference, which is also the translation vector of the co-moving frame K' of the segment. In this case, the relativistic velocity combination [18] gives the following for the radial (r) and orthoradial (o) components of the two wave velocity vectors in K:

$$\left(v_{p/f}\right) r = \frac{v_{0p/f}}{\gamma} \tag{18}$$

$$\left(v_{p/f}\right) o = 2\pi Nr, \tag{19}$$

where $\gamma = \frac{1}{\sqrt{1 - \left(\frac{2\pi Nr}{c}\right)^2}}$ is the Lorentz factor at a distance r from the center.
The radial components of the displacements of the two waves p and f as they travel along the segment can be written in the form: $\mathrm{d}r = (v_{p/f})_\mathrm{r}\mathrm{d}t_{p/f}$. With the equality $\mathrm{d}r = \mathrm{d}r_0$, equation (18), and equation (13) which applies again, the expressions for the two displacements become $\mathrm{d}r_0 = v_{0p/f}.\mathrm{d}t_{0p/f}$. These expressions allow us to obtain in K_0 the expression for the difference in propagation times (defined according to $\mathrm{d}t_0 = \mathrm{d}t_{0p} - \mathrm{d}t_{0f}$): $\mathrm{d}t = \mathrm{d}r_0\left(\frac{1}{v_{0p}} - \frac{1}{v_{0f}}\right)$. Thus, with the difference $\Delta n = n_p - n_f$ between the corresponding refractive indices, the phase difference is expressed by: $\mathrm{d}\phi = 2\pi\nu.\mathrm{d}r_0.\Delta n$. We see that there is only the optical term. We note that for a fiber oriented along a radius of the disk, there is no kinematic contribution to the phase shift between the two secondary waves.
  Thus, for the contribution of a fiber segment which is of arbitrary orientation, only its orthoradial projection is to be taken into account for the kinematic term.

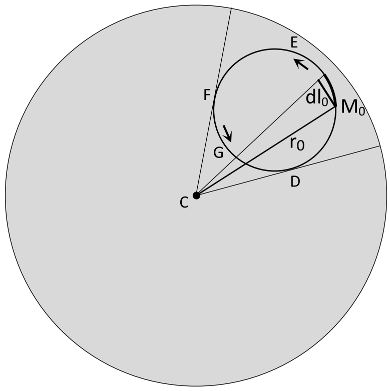

Figure 9. The interferometer as seen from the K_0 reference frame, in which it is at rest, with a turn of one of the three small fiber coils attached to the platform.

Points D and F are the points where two radii of the platform are tangent to the circle. The secondary wave, which travels in the turn in the direction indicated by the arrow at E, travels in the same direction as the rotation of the disk relative to the laboratory frame of reference. After passing point F, this wave is now traveling in the direction indicated by the arrow near G, therefore in the opposite direction to the rotation. There is another reversal of direction at point D. The other secondary wave obviously undergoes the same type of reversal at the same points.

At point M_0, located at a distance r_0 from the center of the disc, there is an infinitesimal element of the circular fiber, with dl_0 being the length of its orthoradial projection. To calculate the difference in travel time between the two secondary waves on one turn of the coil, we need the value of the integral of the product r_0dl_0 over each of the two parts of the turn separated by D and F. To do this, we note that this product is numerically equal to the area of the rectangle constructed on the two segments of lengths r_0 and dl_0, and is therefore equal to twice the area of the triangle, with vertex C, having these two segments as sides. This triangle is also the area swept by a radius vector CM originating from C when M is a moving point travelling along an infinitesimal element of the fiber. Thus, the integral of the product r_0dl_0 over the part FGD of the circle is twice the area of the geometric sector CFGDC. Similarly, the integral over the other part DEF of the circle is twice the area of the previous sector CFGDC plus the small disk.

- The previous remark facilitates the study of the case of the three excess fibers wound on the platform as small coils of a few turns. A circular turn of such a coil is shown in figure 9. Let us consider any infinitesimal portion of the turn, such as the one in figure 9 located at a distance r_0 from the center of the disk. Its contribution to the time difference is given by equation (14), where we retain only the kinematic part and replace R with r_0:

$$\mathrm{d}t_0 = \left(\frac{4\pi N}{c^2}\right) r_0 \mathrm{d}l_0 \tag{20}$$

Since only the orthoradial projection of a fiber element contributes to the difference between the two propagation times of the two secondary waves, the term $\mathrm{d}l_0$ in equation (20) must therefore represent the length of the orthoradial projection of the element, as shown in figure 9. To obtain the difference in travel time of one identified secondary wave relative to the other wave, we must calculate the integral of $\mathrm{d}t_0$ over the loop, and thus the integral of the product r_0dl_0. However, in this regard, we must take into account the changes, at points D and F, in the relative directions of circulation indicated in figure 9. Thus, if the integral over the DEF curve is considered positive, the integral over the FGD curve must be considered negative. It follows from the information in the caption of figure 9 that the integral of the product r_0dl_0 is equal to twice the area of the small disk. We know that in the case of our interferometer, all radial lengths have the same values in K_0 (non-inertial) and in K (inertial), but also that the orthoradial lengths in fact differ only by a Lorentz factor equivalent to one. Under these conditions, the area of the loop in K_0 is still given by πr^2, where r is its radius in either frame of reference. Let b denote b the number of turns, equation (5) leads to the phase shift created between the two secondary waves in the small coil:

$$\Delta\phi = \frac{16\pi^3 \nu N r^2 b}{c^2}. \tag{21}$$

Let us compare the see that there is only the optical coils. With $r = 3$ cm, $b = 4$, $R = 15$ cm, $B = 107$, the ratio of their kinematic phase shifts reduces to $R^2B/r^2b \approx 670$. The effect of the small coils is very small in comparison.

- Let us now consider the polarization modifier whose coil is perpendicular to the plane of the platform. One of its turns is shown in figure 10. Any infinitesimal element of this turn has, in addition

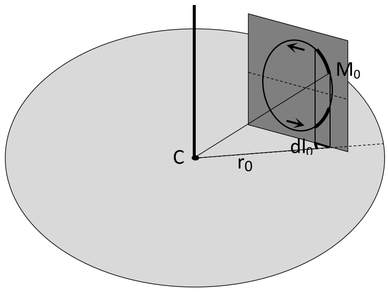

Figure 10. Representation of a fiber turn of the polarization modifier.
It is located in a plane perpendicular to the interferometer platform. The upper half of the turn is distinguished from the lower half. The two arrows indicate the direction of propagation of one of the two secondary waves. In one half of the turn, the direction is the same as the rotation of the platform relative to the laboratory frame of reference, and it is opposite in the other half of the turn. An infinitesimal fiber element located at point M_0 is highlighted, as well as its symmetrical counterpart on the lower half of the turn. The length r_0 is that of the projection of the radius vector CM_0 onto the platform. The two projections onto the platform of the two turn elements overlap, and each can be decomposed into a radial component and an orthoradial component of length $\mathrm{d}l_0$.

to the radial and orthoradial components, a component parallel to the axis of rotation. Since this component is perpendicular to the velocity vector associated with the rotation of the interferometer, it does not induce a Sagnac effect. The orthoradial components remain the only ones to be considered in equation (20) for calculating the kinematic phase shift. Figure 10 shows the length $\mathrm{d}l_0$, which is relevant for both of the two identified fiber elements. The two secondary waves exhibit a certain propagation time difference $\mathrm{d}t_0$ on the upper fiber element. According to the legend in figure 10, on the lower fiber element, the waves have, by comparison, exchanged their directions of propagation relative to the rotation of the interferometer. As a result, the propagation time difference on this fiber element is $-\mathrm{d}t_0$. Since each turn is composed of such symmetrical pairs of elements, there is no phase shift created by the polarization modifier coil.

- Finally, there are a few short fiber segments on the platform that connect the elements. Based on the preceding calculations, we know that the associated kinematic phase differences depend on the spatial orientations on the platform and the lengths. Their projected orthoradial lengths are on the order of a few centimeters; given the 100-meter fiber length of a large coil, the phase difference values involved are also numerically negligible.

Appendix B. Reciprocal and non-reciprocal effects

We speak of a non-reciprocal effect when the characteristics of a wave are affected differently depending on whether it propagates in one direction or the other. Sagnac effect and effects related to the shape of the fiber are not the only possible ones. Consider the example of a short-duration disturbance in the fiber, for example, 1 μs, on a short section located at one end of the coil. This could be a local compression, or a temperature rise, which will transiently affect the values of the refractive index or the absorption coefficient, and consequently affect the characteristics of the two waves propagating through it at that instant. For the wave that has already traveled the length of the coil, the disturbed portion reaches the detector first. For the other wave, the disturbed portion only arrives after it has traveled the entire length of the coil, a journey that lasts approximately 1 μs for a 200-meter coil. The detector therefore initially receives a disturbed wave and an undisturbed wave, then the roles are reversed between the two waves. At the detector level, the two waves are not affected in the same way. This phenomenon can persist if the disturbance is caused by a persistent vibration.

Conversely, in the example of the power emitted by the laser diode decreasing over time, this affects both secondary waves equally. There is indeed an effect in the detector, but it is a reciprocal effect.

The literature on FOG lists other non-reciprocal effects related to certain interferometer components through which both waves propagate in opposite directions [25]. When the goal is to produce a high-precision instrument by exploiting the Sagnac effect, it is essential to identify and reduce all non-reciprocal effects that could be superimposed on it.

Appendix C. Some chronological milestones regarding the relativist interpretation of the Sagnac effect.

In the 19th century, various hypotheses were considered regarding the mode of propagation of light in transparent matter. According to the theories in question, the speed would be determined:

– Entirely by the speed of the source (emission theory),
– By a propagation medium specific to light, the Aether, which would be fixed in a particular frame of reference, and present in transparent matter regardless of its state of motion (theory of the stationary Aether)
– By the Aether, but this would be locally driven by the moving matter, either completely driven (it has the same speed as the matter), or partially (its speed is a fraction of that of the matter).

According to the macroscopic theory currently in use, the propagation of light results from the interaction between the incident light and the different parts of the transparent matter, each of which re-emits light with a certain phase shift; this determines a certain speed for the composite wave, composed of all these contributions, relative to the matter [6] (chapter 4). Furthermore, the choice of a kinematic to switch to another frame of reference is an independent question.

1810. François Arago measured the angles of deflection of light rays from a star using a prism. When the Earth was moving towards the star, the speed of light in the prism had a certain value. Six months later, since the Earth was moving away from the star, the speed in the prism should have been lower, based on the assumption that the speed is determined by the motion of the source (emission theory). And, since the refractive index of the prism depends on the speed, this should affect the angle of deflection, but he found no significant difference. The measurements having been carried out with the greatest possible precision for the time, he asked A. Fresnel to provide him with a theoretical model capable of explaining his results.

1818. Augustin Fresnel, based on ad hoc hypotheses, proposed his theory of the Partial Aether Dragging in agreement with Arago's observations. According to this theory, the velocity, which would be c/n if the medium of index n were at rest in the Aether, is increased by the quantity $(1–1/n^2)v$ when the medium has a velocity v.

1851. Hippolyte Fizeau set up an experiment to test Fresnel's theory using an interferometric method. He circulated water at high speed through a U-shaped tube. Two secondary beams of light interfered, one propagating through the water in the direction of its movement and the other propagating in the opposite direction. The experimental results were in good agreement with Fresnel's formula.

Until the early 20th century, Fresnel's formula coexisted with several microscopic theories of the mechanisms of light propagation in media (G. Sagnac had one).

1907. Max Von Laue, after A. Einstein had defended the scheme of relativistic kinematics and an electromagnetic theory without Aether, reconsidered Fresnel's formula. He showed that, for a wave propagating in a translating medium, the relativistic law of velocity composition can be written in terms of the refractive index in a form that is identical to Fresnel's formula when the speed of the medium is small compared to c (which is the case for typical experiments). Relativity thus incorporates Fresnel's formula without postulating either dragging or the Aether itself.

1911. Max Von Laue showed that, in the case of a slowly rotating interferometer with two waves propagating in opposite directions in a vacuum, classical and relativistic kinematics lead to practically the same interference effect.

1913. Georges Sagnac demonstrated a phase shift between two secondary waves circulating in the air (equivalent to a vacuum), between mirrors. All the equipment—the source, the mirrors, and the photographic detector—was fixed on a rotating platform.

On a theoretical level, G. Sagnac did not subscribe to relativist interpretations.

1920. Max Von Laue demonstrated that, in the case of a rotating interferometer with two waves propagating in opposite directions in a medium of arbitrary refractive index, according to relativistic kinematics, the difference in propagation times is proportional to the angular velocity and independent of the refractive index.

Various experiments over the years have addressed this case study. When the first optical fibers appeared in the 1970s, the manufacture of precision fiber optic gyroscopes became a possibility. The theory of relativity is an integral part of this industrial activity.

For historical information at various levels of detail, one can, for example, consult the documents cited in [26].

ORCID iD

Sylvain Fautrat 0009-0002-2294-6529

References

[1] Gourgoulhon E 2013 *Special Relativity in General Frames* (Springer) p §13.6 Sagnac Effect

[2] (NOTE) fiber ring interferometer (FRI) refers to the basic structure of the interferometer. fiber optic gyrocope (FOG) refers to devices intended to study and measure rotational movements from FRIs. I-FOGs are those which exploit the interference phenomenon for this purpose. There are also R-FOGs which instead generate and exploit a resonance phenomenon. This phenomenon is even involved in the very process of emitting light in gyrolasers, in which the material, forming a single loop, is also the site of a laser effect

[3] HC Lefèvre 2014 *The Fiber-Optic Gyroscope* (Artech House, Boston/London)

[4] (NOTE) Component specifications1) FP laser diode: 1310 nm, $\Delta\lambda = 3$ nm, 2 mW, isolator, monitoring output, pigtailed with SMF fiber and FC/APC connector. A 1.5 V battery powers the laser diode, with a 200 Ω trimmer in series, used to adjust the emitted power. 2) Coupler: 2X2 FBT splitter- 50/50 (3dB), 1310 nm, pigtailed with SMF fiber and SM-FC/APC connectors. 3) Fibers: two lengths of approximately 100 meters in loose tube (diameter 900 μm), withE2000/APC connectors, andE2000/APC to FC/APC adapters. 5(& 6) Photodiode: inGaAs PIN, area: diameter 0.5 mm, with FC/APC connector.Transimpedance amplifier: op amp TLC 271 CP, with an adjustable 50 kΩ trimmer, powered by a 9 V battery. When the received optical power is at its maximum expected values, the output is set to approximately 5 V. 7) Displays: large and small voltmeters 0–200 mV, resolution 0,1mV, both powered by the same 9 V battery. The large one is connected to the detector amplifier through a 500k Ω trimmer used as a voltage divider. The small one is connected to the lazer diode monitoring in the same manner. 8) Buzzer: it sounds when the voltage reaches 900mV. It is not connected directly to the detector amplifier. In order to not disturb the voltage, there is first a voltage follower amplifier (op amp TLC 271 CP) and then a voltage amplifier (same op amp TLC 271 CP; 1.5 k Ω; trimmer 50 k Ω). This dual-amplifier is powered by a 9 V battery

[5] Ref. 3, p72

[6] Hecht E 2017 *Optics* 5th edn (Pearson) pp §5.6,§8.4

[7] Ref. 3, p303.

[8] Ref. 3, p304.

[9] (NOTE) Polarization controllers with pivoting fiber loops (Lefèvre controllers) take advantage, in a calibrated manner, of the effect on the polarization direction

[10] Andronova I A, Gelikonov G V and Malykin G B 1999 Characteristic features of the effects of polarization nonreciprocity" of fiber ring interferometers *Quantum Electron.* **29** 271–5;
Malykin G B and Pozdnyakova V I 2004 Geometric phases in singlemode fiber lightguides and fiber ring interferometers *Phys.-Usp.* **47** 289–308;
Malykin G B and Pozdnyakova VI 2013 *Ring Interferometry* (De Gruyter)

[11] (NOTE) The series with V = 0 at rest was obtained by predetermining regularly spaced rotational speed values. Therefore, the extrema found in the measurements are unlikely to coincide perfectly with the actual extrema of the quantity. Conversely, in the other series, the extrema were specifically sought during the measurements

[12] (NOTE) It is recalled that the phase velocity is considered to be entirely determined at each point by the propagation medium (the fiber)

[13] Malykin G B 2000 The Sagnac effect: correct and incorrect explanations *Phys.-Usp.* **43** 1229–52

[14] Rizzi G and Ruggiero M L 2004 The relativistic Sagnac effect: two derivations *Relativity in Rotating Frames* ed G Rizzi and M L Ruggiero (Springer) pp 179–220

[15] Ref. 1, §13.3–5

[16] Kumar J 2024 Ehrenfest paradox: a careful examination *Am. J. Phys.* **92** 140–5

[17] Rindler W 2006 *Relativity: Special, General, and Cosmological* 2d edn (Oxford University Press) pp §3.3

[18] Ref. 17: §3.6

[19] Ref. 17: §3.5

[20] (NOTE) In the literature on the Sagnac effect, relativistic phase-shift calculations are most often performed by considering two waves with the same local speed: $v_{0+} = v_{0-} = v_0$. In this case, the "optical" contribution to the time difference and the phase shift does not appear. For the theoretical analysis, which here focuses on experimental observations including birefringence effects, the calculations must be generalized. (In reference 15, the calculation is initially performed with two different speeds but is then simplified.) Furthermore, the generalized calculation has the conceptual advantage of clearly demonstrating the independent nature of the kinematic and optical contributions

[21] (NOTE) The frequency ν is measured in the K_0 frame of reference where the transmitter is located. However, a wave observed from a rotating disk has a frequency value that changes during its propagation like the Lorentz factor, depending on the distance from the center. More precisely, if its frequency at the center is $\nu(0)$, its frequency at a point at a distance r is $\nu(r) = \gamma(r).\nu(0)$. (This relationship is obtained from the period of the wave at each point of the disk, which is identified with an infinitesimal

proper time that itself follows the law of dilation.) For the interferometer under study, all values of $\gamma(r)$ involved are equivalent to unity, and there is no need to distinguish numerically between the different frequency values.

[22] Lefèvre H C 2014 The fiber-optic gyroscope, a century after Sagnac's experiment: the ultimate rotation-sensing technology? *Compt. Rendus Phys.* **15** 851–8

[23] Ref. 10

[24] Ref. 3

[25] Andronova I A and Malykin G B 2002 Physical problems of fiber gyroscopy based on the Sagnac effect *Phys.-Usp.* **45** 793–817

[26] Malykin G B 1997 Earlier studies of the Sagnac effect *Phys.-Usp.* **40** 317–21;
Anderson R, Bilger H R, Stedman G E 1994 Sagnac effect: a century of Earth-rotated interferometers *Am. J. Phys.* **62** 975–985;
Darrigol O 2012 *A History of Optics from Greek Antiquity to the Nineteenth Century* (Oxford University Press) ch 6; Darrigol O 2014 Georges Sagnac: A life for optics *C. R. Phys.* **15** 789–840